INL/EXT-20-59969 Rev. 0

BISON Development and Validation for Priority LWR-ATF Concepts

15 September 2020

Technical Report

Kyle A. Gamble[1], Giovanni Pastore[2], and Michael W. D. Cooper[3]

[1]Idaho National Laboratory
[2]University of Tennessee, Knoxville
[3]Los Alamos National Laboratory

Changing the World's Energy Future

Idaho National Laboratory

BISON Development and Validation for Priority LWR-ATF Concepts

Technical Report

Kyle A. Gamble[1], Giovanni Pastore[2], and Michael W. D. Cooper[3]

[1]Idaho National Laboratory
[2]University of Tennessee, Knoxville
[3]Los Alamos National Laboratory

15 September 2020

Idaho National Laboratory
Computational Mechanics and Materials Department
Idaho Falls, Idaho 83415

http://www.inl.gov

Prepared for the
U.S. Department of Energy
Office of Nuclear Energy
Under U.S. Department of Energy-Idaho Operations Office
Contract DE-AC07-05ID14517

Page intentionally left blank

Abstract

Over the years, the Nuclear Energy Advanced Modeling and Simulation (NEAMS) (2015-2018, 2020) and Consortium for Advanced Simulation of Light Water Reactors (CASL) (2019) programs have provided support for the development of accident tolerant fuel (ATF) material models in the BISON fuel performance code. Since the beginning, the goal has been to utilize a multiscale modeling approach to gain a physical understanding of the fuel concepts of interest and develop mechanistic models in the absence of a large amount of experimental data. This work builds upon that of previous years. In particular, we present newly updated fission gas release models for both gas behavior in both Cr_2O_3-doped UO_2 and U_3Si_2 fuels, as well as a new creep model for U_3Si_2. The validation exercises completed last year are revisited with the latest models and the results updated. A brief summary of recent modeling activities regarding FeCrAl cladding is also provided.

Page intentionally left blank

Acknowledgments

This work was funded by the U.S. Department of Energy under both the NEAMS and CASL programs. This report was authored by a contractor of the U.S. Government under Contract DE-AC07-05ID14517. Accordingly, the U.S. Government retains a non-exclusive, royalty-free license to publish or reproduce the published form of this contribution, or allow others to do so, for U.S. Government purposes.

This research utilized the resources of the High Performance Computing Center at Idaho National Laboratory, which is supported by the Office of Nuclear Energy of the U.S. Department of Energy and the Nuclear Science User Facilities under Contract No. DE-AC07-05ID14517.

Page intentionally left blank

Contents

List of Figures

List of Tables

Acronyms

ATF	accident tolerant fuel
ATR	advanced test reactor
CRP	Coordinated Research Project
CASL	Consortium for Advanced Simulation of Light Water Reactors
FGR	fission gas release
HIP	high-impact problem
IAEA	International Atomic Energy Agency
INL	Idaho National Laboratory
LANL	Los Alamos National Laboratory
LHR	linear heat rate
LHS	Latin hypercube sampling
LWR	light water reactor
MOOSE	Multiphysics Object-Oriented Simulation Environment
NEAMS	Nuclear Energy Advanced Modeling and Simulation
PCMI	pellet-clad mechanical interaction
PIE	post-irradiation examination
PWR	pressurized water reactor

Page intentionally left blank

1. Introduction

An investigation into accident tolerant fuel (ATF) using the BISON fuel performance code [1] has been ongoing since 2015. The work presented this year presents a culmination of a multi-laboratory effort to develop multiscale informed modeling capabilities for the ATF concepts Cr_2O_3-doped UO_2 and U_3Si_2. The reports [2] and [3] provided an overview of the material models available in BISON for the priority fuel and cladding concepts Cr_2O_3-doped UO_2 and U_3Si_2, chromium-coated Zircaloy, and FeCrAl. These reports also included an estimation of the range of applicability and uncertainty associated with the individual models. Since the publication of these reports last year, additional lower length scale work at Los Alamos National Laboratory (LANL) refined some of the models at the engineering scale, including fission gas behavior in both Cr_2O_3-doped UO_2 and U_3Si_2, as well as the development of a creep model for U_3Si_2. Uncertainty in the U_3Si_2 fission gas behavior model was also estimated. Additional parameter refinements for the U_3Si_2 fission gas model were achieved through lower length scale work by other collaborators at Idaho National Laboratory (INL).

This year, the updated models were incorporated into BISON, and the validation analyses completed in last year's reports were revisited. For U_3Si_2 fuel, the sensitivity analysis was also completed for the ATR-ATF experiments [4], taking into account all of the uncertain models while using updated uncertainties.

In regards to ATF cladding concepts, we summarize INL's contribution to an International Atomic Energy Agency (IAEA) benchmark on fuel performance modeling of FeCrAl cladding for which the final report [5] was recently published.

This report concludes with a summary of the work completed this year, as well as an outlook on the multiscale modeling tasks related to ATF concepts going forward. In particular, the focus is on mechanical model improvements for Cr_2O_3-doped UO_2 as U_3Si_2 is no longer being pursued by industry for use in light water reactors (LWRs).

2. Cr_2O_3-Doped UO_2

Cr_2O_3-doped UO_2 fuel is a potentially attractive alternative to traditional UO_2 fuel currently used in LWRs because of its larger grain size possibly reducing FGR. A potential advantage in terms of pellet-cladding interaction (PCI) behavior also exists, which is related to different creep and cracking behaviors compared to standard UO_2. This year, the multiscale modeling's focus was continued refinement of the fission gas behavior in Cr_2O_3-doped UO_2. Lower length scale model developments in the area of creep and cracking behavior are planned for the next fiscal year.

2.1 Fission Gas Behavior Modeling Updates

The general form of fission gas diffusivities in BISON for the lower length scale informed model is given by:

$$D^{doped} = \exp\left(-\frac{\Delta H_1}{k_B}\left[\frac{1}{T}-\frac{1}{T_1}\right]\right) D_1^{undoped} + \exp\left(-\frac{\Delta H_2}{k_B}\left[\frac{1}{T}-\frac{1}{T_2}\right]\right) D_2^{undoped} + D_3^{undoped} \tag{2.1}$$

where k_B is Boltzmann's constant (ev/K), T is the temperature (K) the parameters, and T_1, T_2, ΔH_1, and ΔH_2 are defined in Table 2.1 for both the best estimate (Case A) and the upper limit (Case B). The unperturbed diffusion coefficients, $D_1^{undoped}$, $D_2^{undoped}$, and $D_3^{undoped}$ are given by [6]:

$$D_1^{undoped} = 7.6 \times 10^{-10} \exp\left(\frac{-4.86 \times 10^{-19}}{k_B T}\right) \tag{2.2}$$

$$D_2^{undoped} = 5.64 \times 10^{-25} \sqrt{\dot{F}} \exp\left(\frac{-1.91 \times 10^{-19}}{k_B T}\right) \tag{2.3}$$

$$D_3^{undoped} = 8 \times 10^{-40} \dot{F} \tag{2.4}$$

More details on the atomistic calculations performed when developing the above fission gas diffusivity model are presented in [7]. Using the updated diffusitivies, the BISON validation cases from Halden IFA-677 were revisited. The validation simulations are presented in Section 2.2.

Table 2.1. Diffusivity parameters for Cr_2O_3-doped UO_2. Case A is the best-estimate and Case B is the upper limit.

Parameter	Case A	Case B
$T_1 = T_2$ (K)	1773	1773
ΔH_1 (eV)	0.3198	0.3282
ΔH_2 (eV)	-0.3345	-0.6998

2.2 Validation to Halden IFA-677 Fuel Rod Tests

Carried out from December 2004 to September 2007 over six irradiation cycles, the IFA-677.1 experiment tested the performance of six rods subjected to a high initial rating for Halden Boiling Water Reactor conditions. Two of the rods were supplied by Westinghouse and contained UO_2 fuel doped with Cr_2O_3 and Al_2O_3 in line with their (Advanced Doped Pellet Technology) ADOPT. The rods were instrumented with pressure transducers and fuel centerline thermocouples near the top and bottom of the fuel stack. The resultant FGR was estimated online from the pressure measurements and, in the case of Rod 5 a post-irradiation puncture test. A description of Rods 1 and 5 from IFA-677.1 is given in Table 2.2.

Table 2.2. Fabrication characteristics of IFA-677.1 Rods 1 and 5 simulated in this work [8, 9, 10, 11].

	IFA-677.1 Rod 1	IFA-677.1 Rod 5
Cladding material	Zircaloy-4	Zircaloy-4
Fuel material	UO_2+additives	UO_2+additives
Fill gas	He	He
Total active fuel stack length (mm)	398.6	403.5
Drilled active section length, top (mm)	109.2	111.0
Drilled active section length, bottom (mm)	109.7	111.1
Pellet inner diameter, drilled sections (mm)	1.8	1.8
Pellet outer diameter (mm)	9.13	9.13
Diametral gap (μm)	170	170
Cladding thickness (mm)	0.725	0.725
Cladding outer diameter (mm)	10.75	10.75
Free volume (cm^3)	5.34	5.26
Fill gas pressure (MPa)	1.35	1.35
Fuel Cr_2O_3 content (ppm)	900	500
Fuel Al_2O_3 content (ppm)	200	200
Fuel U-235 enrichment (%)	4.94	4.91
Initial fuel density (kg/m^3)	10690	10700
Fuel average grain radius (μm)	28	22.5

BISON simulations were performed to reproduce the Halden tests using the doped UO_2 fission gas diffusivity models outlined in Section 2.1. Several different variations in fission gas diffusivity were evaluated: (1) the standard UO_2 empirical (Turnbull) model, and (2) Case A and (3) Case B of the multiscale enhanced diffusivity model developed in this work. In all cases, the grain radius was set to the values reported in Table 2.2.

Figure 2.1 shows the measured upper centerline thermocouple temperature from the Halden tests for Rods 1 and 5 (red lines), alongside BISON predictions of the temperatures at the same position using the three different diffusivity models. For Rod 1, the agreement between all BISON cases and the measured data is excellent for the first three cycles. During the following two cycles, BISON overestimates the temperatures by 100 K ($\approx$ 7%). During the final cycle, there is a significant overestimate of 300 K. Similarly, Rod 5 shows an overestimate of the temperature during the final irradiation cycle. This behavior may indicate that the input linear heat rate (LHR) for the calculations, which is based on the Halden data, is affected by inaccuracies during the later portion of the irradiation. Indeed, this issue has been postulated for IFA-677, with inaccuracies in the power data potentially arising following a core configuration change whose effect is not taken into account in the power distribution reconstruction [12, 13]. Additionally, in general, there is an uncertainty of at least 7% in the LHR data. Therefore, the fuel centerline temperature is roughly proportional to the local LHR.

Regardless of the fission gas diffusivity model selected, no significant difference is seen in the BISON simulations for the centerline temperature.

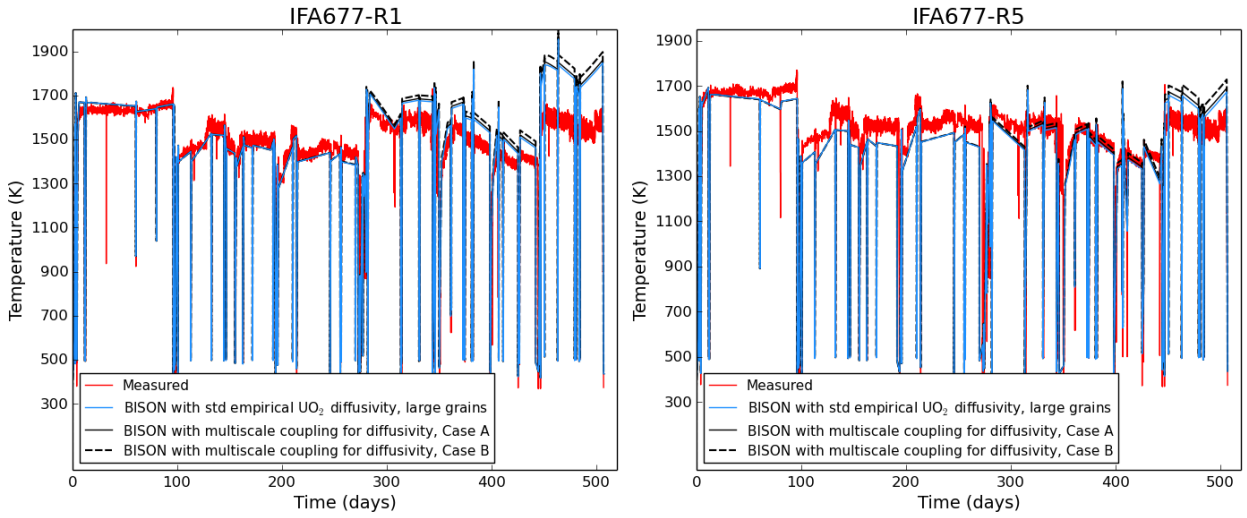

Figure 2.1. The upper thermocouple temperature measured during the IFA-677 test on doped fuel for (a) rod 1 and (b) rod 5 (red lines). BISON results for Case A and Case B using the multiscale enhanced diffusivity model developed in this work are shown by the black lines. Comparison is made to results using the standard empirical undoped UO_2 model with large grains (blue lines).

Figure 2.2 shows the rod pressure as a function of time for Rods 1 and 5. For both rods, reasonable agreement is found between BISON and the experiments. Excellent agreement is found for the BISON simulations using Case A of the multiscale fission gas diffusivity model, while Case B slightly over-predicts the pressure, and the standard undoped UO_2 empirical model with large grains under-predicts the pressure.

FGR as a function of burnup is illustrated in Figure 2.3. A clear difference can be seen between the different fission gas diffusivity models. The standard undoped UO_2 empirical model exhibits the lowest

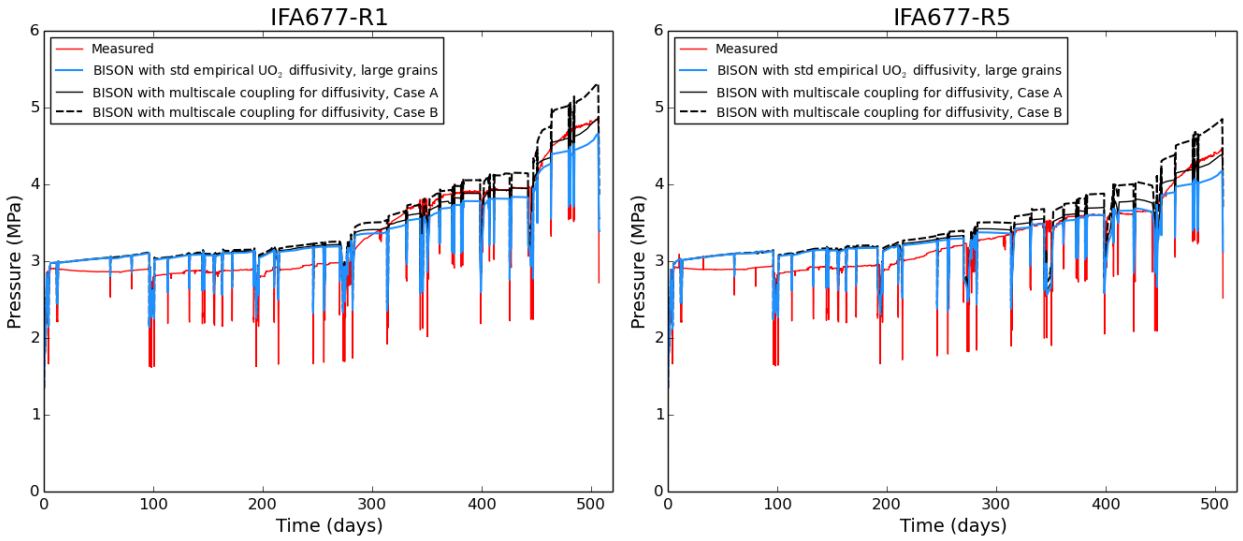

Figure 2.2. The pressure measured during the IFA677 test on doped fuel for (a) Rod 1 and (b) Rod 5 (red lines). BISON results for Case A and Case B using the multiscale enhanced diffusivity model developed in this work are shown by the black lines. Comparison is made to results using the standard empirical undoped UO_2 model with large grains (blue lines).

FGR, since the large grains suppress release and the enhanced diffusivity of other models is not included. As expected, the use of the multiscale fission gas diffusivity model enhances the FGR, given that the enhanced fission gas diffusivity will increase the rate at which gas atoms arrive at the grain boundaries. Case B shows the greatest increase in FGR and gets closest to the experimental results for both Rods 1 and 5. The improvement compared to the baseline standard UO_2 models is significant, highlighting the importance of including enhanced diffusivity and the effectiveness of deploying a multiscale approach. Although the multiscale model results in a significant improvement over the standard UO_2 fission gas diffusivity model, a moderate underestimation of the measured FGR is observed. This indicates that adding Al_2O_3 potentially enhances diffusivity beyond thaht of just adding Cr_2O_3. As was shown in [7] it is impossible to reach oxygen potentials where buffering could occur through the $2/3Al_2O_3 \rightarrow 4/3Al + O_2$ equilibrium. Future work should investigate mechanisms by which additions of Al_2O_3+Cr_2O_3 could result in higher FGR than Cr_2O_3 alone. For example, the formation of an $Al_xCr_{2-x}O_3$ solid solution may result in a slightly different oxygen buffering equilibrium through the reduction of the solid solution to form Cr metal and a more Al-rich oxide. Consequently, the oxygen potential of (Al,Cr)-doped UO_2 is expected to be slightly different when compared Cr-doped UO_2.

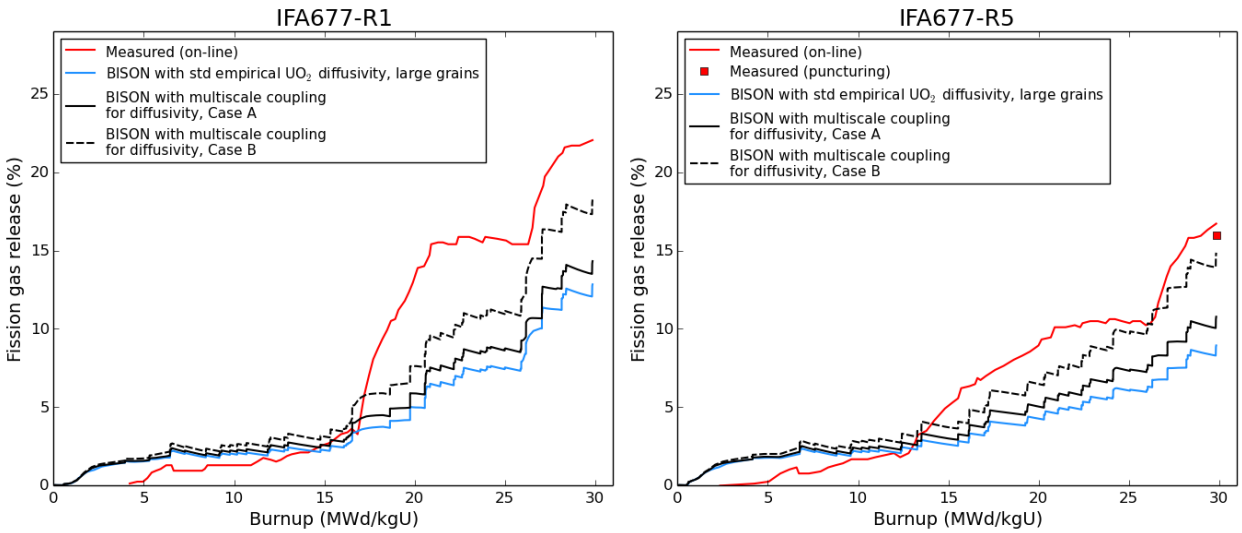

Figure 2.3. The measured FGR during the IFA-677 test on doped fuel for (a) Rod 1 and (b) Rod 5 (red lines). BISON results for Case A and Case B using the multiscale enhanced diffusivity model developed in this work are shown by the black lines. Comparison is made to results using the standard empirical undoped UO_2 model with large grains (blue lines).

3. U_3Si_2 Fuel

U_3Si_2 fuel was a concept being pursued by Westinghouse for use in LWRs to improve accident tolerance and economics. The main advantages are the much higher thermal conductivity and uranium density compared to UO_2. At INL, the Computational Mechanics and Materials team has been developing capabilities to predict U_3Si_2 fuel behavior during both normal operating and accident conditions. This year, multiscale modeling work begun in earlier years finally came to completion. While U_3Si_2 is not pursued anymore for use in LWRs, the multiscale modeling approach used can be applied to any new fuel concepts where limited experimental data is available.

In this chapter, updates to the fission gas behavior model and the development of a lower length scale informed creep model is presented. The uncertainty quantification and sensitivity studies completed last year [2] are revisited using the latest models and their updated uncertainty ranges.

3.1 Fission Gas Behavior Updates

The computational framework for computing the evolution of fission gases during irradiation in U_3Si_2 was developed by [14] and summarized in [2]. The model utilized theoretical values for some parameters, as well as lower length calculations for others. Since the model was original developed, additional lower length scale calculations have been completed to more accurately determine certain parameters. The parameters that were determined to have updated values and uncertainty include, saturation coverage ($F_{c,sat}$), surface energy, the bubble semi-dihedral angle, and the diffusion coefficients for fission gas atoms and vacancies. The saturation coverage value was determined to be 0.6 $\pm$ 0.072 [15]. The surface energy was calculated to be 1.0 $\pm$ 0.5 [16]. Also based on [16], an improved estimate for the semi-dihedral angle of lenticular grain-boundary fission gas bubbles, θ, was calculated to be $\theta = 73°$. Updates to the diffusion coefficients were determined by [17] for both stoichiometric and Si-rich U_3Si_2 microstructures. For fission gas atoms (Xe), the diffusivities are given by:

$$D = \begin{cases} 2.85 \times 10^{-4} \exp\left(\frac{-3.17}{k_B T}\right) + 3.58 \times 10^{-42} \dot{F} & \text{Stoichiometric} \\ 7.22 \times 10^{-6} \exp\left(\frac{-2.84}{k_B T}\right) + 3.58 \times 10^{-42} \dot{F} & \text{Si-rich} \end{cases} \tag{3.1}$$

where $\dot{F}$ is the fission rate density (fissions/m^3-s), k_B is the Boltzmann constant (eV/K), T is the temperature (K), and D is the diffusivity (m^2/s). For vacancies, the diffusivities are given by:

$$D = \begin{cases} 9.40 \times 10^{-4} \exp\left(\frac{-4.17}{k_B T}\right) + 3.01 \times 10^{-47} \dot{F} & \text{Stoichiometric} \\ 9.76 \times 10^{-5} \exp\left(\frac{-4.22}{k_B T}\right) + 3.01 \times 10^{-47} \dot{F} & \text{Si-rich} \end{cases} \tag{3.2}$$

3.2 Lower Length Scale informed Creep Model

Prior to this,d work the creep models for U_3Si_2 were empirical correlations (see [18, 19]) fit to the only experimental data available, which came out of the University of South Carolina. Atomistic calculations were performed at LANL to develop a creep model containing contributions from three creep mechanisms: Coble, Nabarro-Herring, and dislocation climb. The details on the derivation of the creep model can be found in [17]. Here, the final equations as implemented into BISON are shown. The total creep rate is given by:

$$\dot{\epsilon} = \dot{\epsilon}_{NH} + \dot{\epsilon}_{Coble} + \dot{\epsilon}_{Climb} \tag{3.3}$$

where $\dot{\epsilon}_{NH}$, $\dot{\epsilon}_{Coble}$, and $\dot{\epsilon}_{Climb}$ are the contributions from Nabarro-Herring, Coble, and dislocation climb, respectively (s^{-1}). The Nabarro-Herring creep rate is given by:

$$\dot{\epsilon}_{NH} = \frac{\sigma}{d^2}\left[3.023 \times 10^{-15} \exp\left(\frac{-3.246}{k_B T}\right) + 6.812 \times 10^{-54} \dot{F} \exp\left(\frac{-0.5179}{k_B T}\right) + 2.59 \times 10^{-17} \exp\left(\frac{-3.330}{k_B T}\right)\right] \tag{3.4}$$

where σ is the effective stress (Pa), T is the temperature (K), d is the grain size (m), and $\dot{F}$ is the fission rate density (m^3/s). Similarly, the Coble creep rate is given by:

$$\dot{\epsilon}_{Coble} = \frac{\sigma}{d^3} 2.280 \times 10^{-24} \exp\left(\frac{-1.381}{k_B T}\right) \tag{3.5}$$

For dislocation climb, the creep rate is:

$$\dot{\epsilon}_{Climb} = \sigma^3\left[3.444 \times 10^{-15} \exp\left(\frac{-4.02}{k_B T}\right) + 3.759 \times 10^{-58} \dot{F} \exp\left(\frac{-0.0178}{k_B T}\right)\right] \tag{3.6}$$

The newly developed model predicts significantly higher creep rates than the existing empirical correlations of [18] and [19]. To illustrate the effect of U_3Si_2 creep under reactor operating conditions, two analyses of a 10 pellet rodlet are considered, one with no creep activated (i.e., the fuel is treated as elastic) and a second in which the newly developed creep model is activated. The geometry of the rodlet is represented using a 2D-RZ axisymmetric assumption with a smeared fuel pellet column (i.e., dishes and chamfers are not explicitly modeled). Given that the thermal conductivity of U_3Si_2 is so high [20] and the athermal term in equations 3.4–3.6 is so small, virtually no creep is observed at nominal operating linear powers (e.g., 20–25 kW/m). Thus, in this study, the linear power supplied to the fuel is ramped up over 10,000 seconds from 0 to 35 kW/m and held for ∼2.54 years to observe a still, minute effect due to creep.

Figure 3.1 presents both the time history of the fuel centerline temperature as well as the predicted fuel outer diameter at the end of the simulation. One observes that the end-of-life diameter is slightly larger ($<$ 0.01 mm) in the case with creep indicating that computing creep results in an observable but ultimately negligible effect on the final fuel diameter. Similarly, the larger fuel diameter results in a lower average centerline temperature.

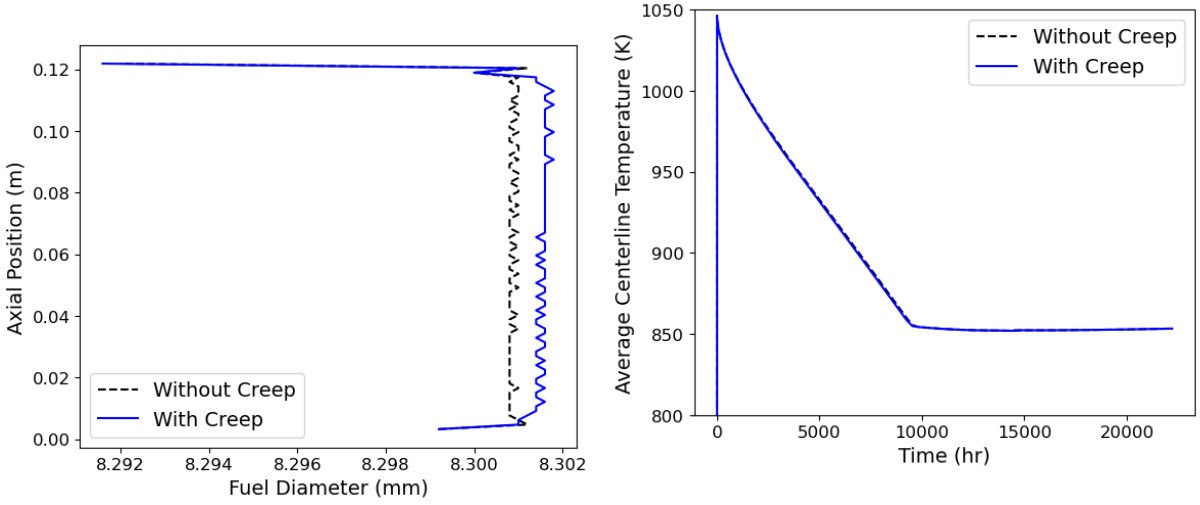

(a) (b)

Figure 3.1. The (a) end-of-life diameter of the fuel and (b) the time history of the average centerline temperature.

After the base irradiation, the fuel rod is subjected to a temperature transient applied to the cladding outer surface that is consistent with furnace tests completed at Studsvik. The peak temperature evolution is provided in Figure 3.2. A sinusoidal profile with values 20 K lower at the ends of the fuel rod (to drive clad ballooning at the center of the rod) is applied.

The creep strain in the fuel is plotted at the point of cladding failure during the transient in Figure 3.3. It is observed that limited creep has occurred throughout the base irradiation and the subsequent transient. The temperature during the transient at the point of failure is ~1100 K, which is still much too low for significant creep to occur. The results are shown at the point of cladding failure because, after this point, the pressure within the rodlet is set equal to the atmospheric pressure on the outside of the rod, effectively eliminating any driving force of creep even as the temperature continues to climb. It is suspected that the only accident in which U_3Si_2 creep becomes a factor is during a station blackout when the rod remains pressurized as the temperatures rise.

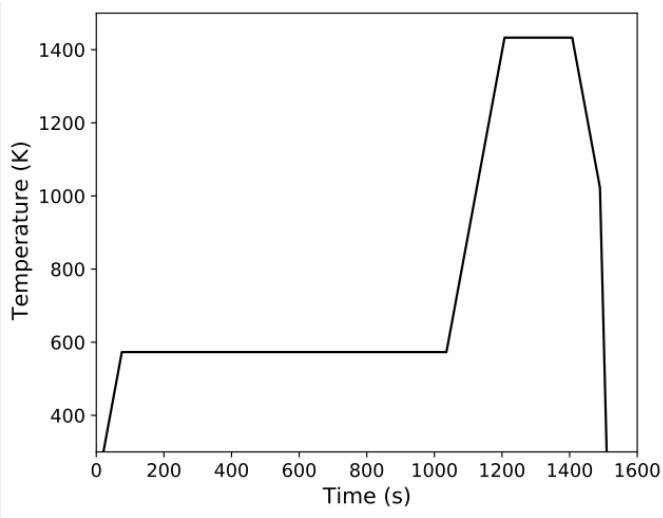

Figure 3.2. The cladding temperature prescribed during the LOCA transient.

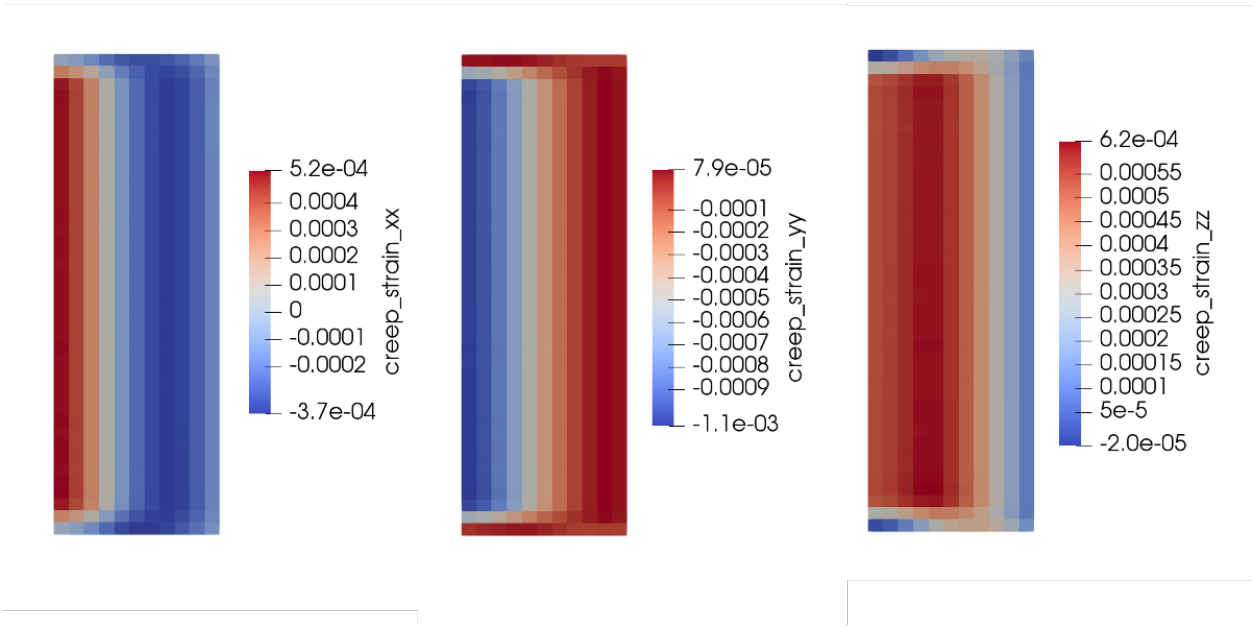

Figure 3.3. The creep strain in the (a) radial, (b) axial, and (c) hoop directions within the fuel at the time of cladding failure during the transient.

3.3 Validation

The only experimental data available to validate the U_3Si_2 models in BISON are from the two rods that underwent post-irradiation examination (PIE). PIE was completed on the two rods identified as R4 from

the ATF-13 capsule and R6 from the ATF-15 capsule [4]. The experiments are a typical capsule irradiation test, consisting of a fuel rodlet encapsulated inside of a stainless steel capsule. The nominal dimensions of all capsules used in the ATF-1 experiments are shown in Figure 3.4. Specific details for the R4 and R6 rodlets can be obtained from the design specifications of the experiments. The R4 and R6 rodlets consisted of 12 enriched (5.44 wt% U-235) U_3Si_2 pellets stacked on top of a single depleted pellet, with an additional two depleted pellets placed on top of the active length. The top two depleted pellets were drilled to accommodate melt wires for monitoring the temperature during the experiments. In these experiments, the fuel was placed inside ZIRLO^{TM} before being inserted into the stainless steel capsule. Details on the fabrication of the fuel pellets are discussed by [21].

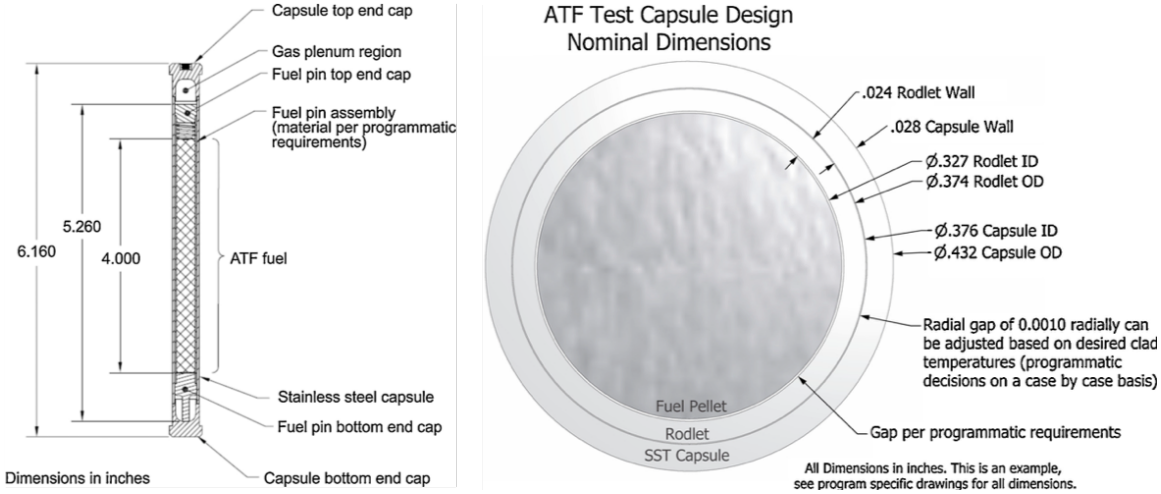

Figure 3.4. ATF-1 test capsule assembly (left) and capsule cross-section (right). Images reproduced from Barrett et al. [22].

The power supplied to the fuel rodlets as a function of time is shown in Figure 3.5. A flat axial profile was assumed in the BISON simulation, given the short length of the rodlet. The rodlets were removed from the ATR at a relatively low burnup (17.1 MWd/kgHM for R4 and 19.6 MWd/kgHM for R6 [4]) to perform PIE. For engineering scale simulation comparisons, limited data exists. Previous experience from research reactor irradiations of U_3Si_2 suggested that, at some point, the fuel will experience runaway swelling [23]. Therefore, measurements focused on dimensional changes of the fuel and cladding, as well as FGR. Measurements of fuel dimensional changes were limited to neutron radiography, which illustrated the fuel experienced no axial growth (elongation) to the resolution of the measurement technique. Cladding profilometry measurements indicated negligible change from the as-fabricated dimensions, meaning that no contact between the fuel and cladding was observed.

A full uncertainty quantification (UQ) and sensitivity study was completed. Table 3.1 presents the range of applicability, uncertainty and references for all of the U_3Si_2 models available in BISON. The uncertainties are assumed to represent two standard deviations for the normal and lognormal distributions. For the uniform distributions, any and all values between the upper and lower limits of the range are possible. In

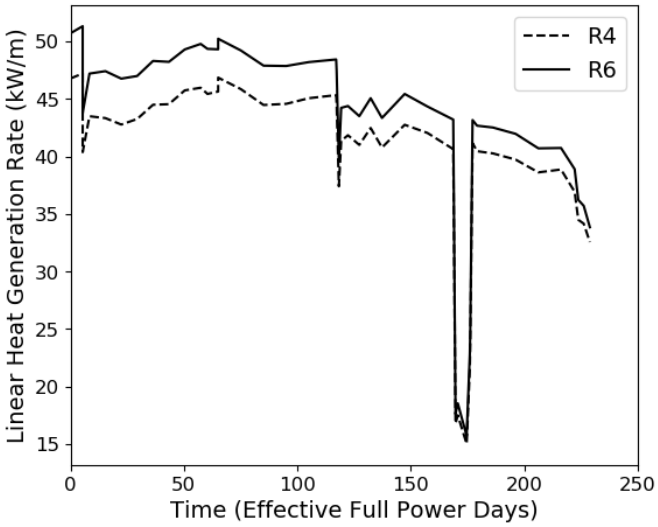

Figure 3.5. Linear heat generation rate supplied to ATR-13 R4 and ATR-15 R6. Adapted from Cappia and Harp [4].

the table, T is the temperature, and p is the porosity. Further details on the form of the equations and the determination of their uncertainty can be found in [2]. It should be noted that, based on [24] that grain growth of U_3Si_2 can be ignored. In addition, since the mechanism of densification will be different in U_3Si_2 compared to UO_2 it was neglected in this study, contrary to previous investigations [2, 25].

Table 3.1. Summary of U_3Si_2 models available in BISON, including range of applicability, uncertainty, and the distribution used in the uncertainty quantification and sensitivity analyses of the validation cases.

Model	Range of Applicability	Uncertainty	References	Distribution
Thermal conductivity	13 K $\leq T \leq$ 1500 K	$\pm$ 18.2%	[20]	Normal
Specific heat capacity	293 K $\leq T \leq$ 1500 K	$\pm$ 3%	[20]	Normal
Young's modulus	1.5% $\leq p \leq$ 10%	$\pm$ 29.1%	[20]	Normal
Poisson's ratio	1.5% $\leq p \leq$ 10%	$\pm$ 26.8%	[20]	Normal
Thermal expansion	273 K $\leq T \leq$ 1473 K	$(16.0 \pm 3.0) \times 10^{-6}$	[20]	Normal
Solid swelling	All burnups	$\pm$ 20%	[26, 27]	Normal
Xe and vacancy diffusion thermal coefficients	Normal operating conditions	Factor of 7.4		Uniform
Xe and vacancy thermal activation energies	Normal operating conditions	$\pm$ 0.15 eV		Uniform
Xe and vacancy athermal coefficients	Normal operating conditions	Factor of 5		Uniform
Fission gas release and gaseous swelling	Normal operating conditions	[1]Factor of 10^{-3} to 10^4	[14]	Lognormal
	Normal operating conditions	[2]Factor of 0.1 to 10	[14]	Uniform
	Normal operating conditions	[3]$\pm$ 50%	[14]	Uniform
	Normal operating conditions	[4]Factor of 10^{-3} to 10^3	[14]	Lognormal
	Normal operating conditions	[5]Factor of 0.5 to 1	[14]	Uniform
	Normal operating conditions	[6]0.6 $\pm$ 0.072	[14]	Normal

[1]Applied to nucleation factor of intragranular bubbles. [2]Applied to the re-solution rate of intra-granular bubbles. [3]Applied to the U_3Si_2/gas specific surface energy. [4]Applied to the initial number density of intergranular bubbles. [5]Applied to the semi-dihedral angle of intergranular bubbles. [6]Applied to the saturation coverage of grain boundaries.

To perform the study, a finite element mesh of the drop-in capsule was created using a 2D-RZ axisymmetric smeared pellet mesh assumption. This means that there is an azimuthal plane of symmetry about the rodlet centerline, and the dish and chamfer features of the fuel are not modeled. The insulator pellets, one at the bottom of the stack and two at the top, were included in addition to the ZIRLO^{TM} cladding and stainless steel capsule. Eleven finite elements were used through the radius of the fuel pellet, with four each through the thickness of the cladding and capsule. Three axial elements per pellet were used with the cladding, and the capsule meshes being slightly coarser to ensure improved robustness of the contact algorithm.

The uncertainty quantification and sensitivity analysis studies were performed by coupling BISON to the Dakota [28] software developed at Sandia National Laboratories. A Latin hypercube sampling (LHS) technique was used to reduce the number of samples required. Two-thousand samples were run for two separate studies, the first using the stoichiometric diffusivities for Xe atoms and Si vacancies and the second using the Si-rich diffusivities. The results of the study are presented in Table 3.2 and Figures 3.6 and 3.7.

Table 3.2 presents the results of the uncertainty quantification analysis. The BISON results are presented as the minimum to maximum value of fuel elongation and FGR assuming two standard deviations about the mean value. The reason the minimum and maximum values were chosen to be reported is because the lower value for FGR would be negative, which is non-physical. The results indicate that BISON predicts a small, non-zero axial change in the fuel stack. While the uncertainty range does not encompass the experimental measurement of zero axial change, it should be noted that the uncertainty of the neutron radiography technique is likely large enough to overlap with the uncertainty of the model predictions. In addition, recall that a densification model was not included in the BISON analyses due to the unknown nature of the mechanism in U_3Si_2. If such a model were added, it would serve to reduce the total amount of fuel elongation.

Figures 3.6 and 3.7 illustrate the Spearman correlation coefficients for the stoichiometric and Si-rich fission gas diffusivities, respectively. Spearman correlation coefficients were chosen because some of the uncertain inputs have orders-of-magnitude variation. These coefficients can identify monotonic relationships between inputs and outputs and are always between -1.0 and 1.0. A larger negative value indicates that, as the uncertain input is increased, the corresponding output of interest decreases. Conversely, a larger positive value indicates a positive monotonic relationship between the input and output. A correlation value close to 0.0 indicates no monotonic relationship. A statistically significant relationship between the input and output is assumed to occur when the absolute value of the correlation coefficient is greater than 0.33.

It is observed that the trends of the Spearman correlation coefficients are the same whether or not the diffusivities used for the fission gas atoms and vacancies in the fission gas model are treated as stoichiometric or Si-rich. One sees a moderate effect due to the power (and correspondingly temperature) differences between Rods R4 and R6 (e.g., thermal conductivity and the coefficient of thermal expansion). The most significant relationships with fuel elongation are the vacancy and Xe diffusion activation energies, vacancy and Xe diffusion thermal coefficients, the solid swelling factor, the Young's modulus, and the coefficient of thermal expansion. For FGR the significant input parameters are the intragranular nucleation factor,

intergranular bubbles dihedral angle, re-solution rate, and the coefficient of thermal expansion. Performing additional lower length scale calculations or separate effects experiments for these parameters will help reduce the uncertainty in the inputs and correspondingly improve the predictions of the outputs of interest.

Table 3.2. BISON comparisons to PIE data for ATF-13 R4 and ATF-15 R6 [29].

	BISON				Experiment	
	R4		R6		R4	R6
	Stoichiometric	Si-Rich	Stoichiometric	Si-Rich		
Fuel elongation (mm)	0.178 to 0.256	0.159 to 0.235	0.272 to 0.410	0.226 to 0.364	0.0	0.0
Fission gas release (/)	0.0 to 0.006	0.0 to 0.002	0.002 to 0.016	0.0 to 0.0121	0.0006	0.0006

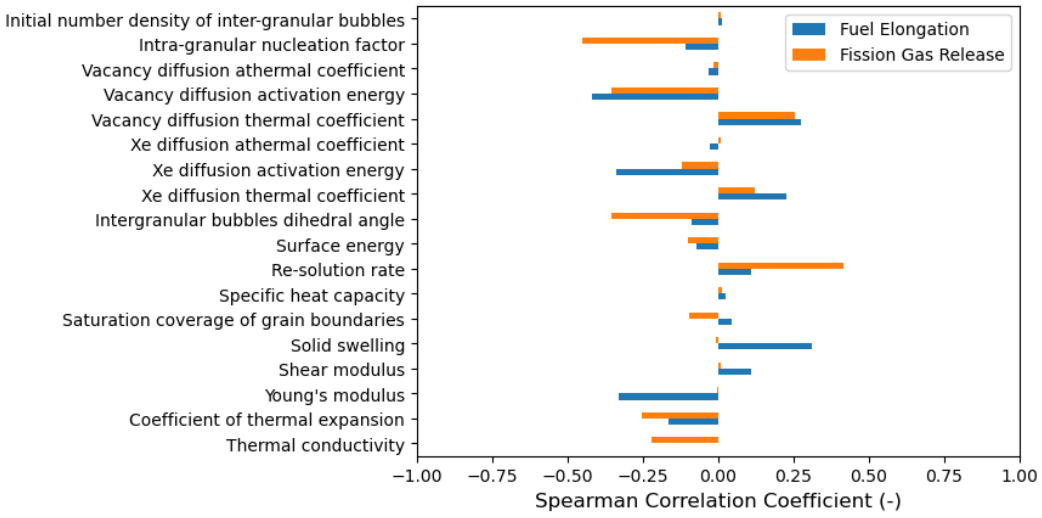

(a)

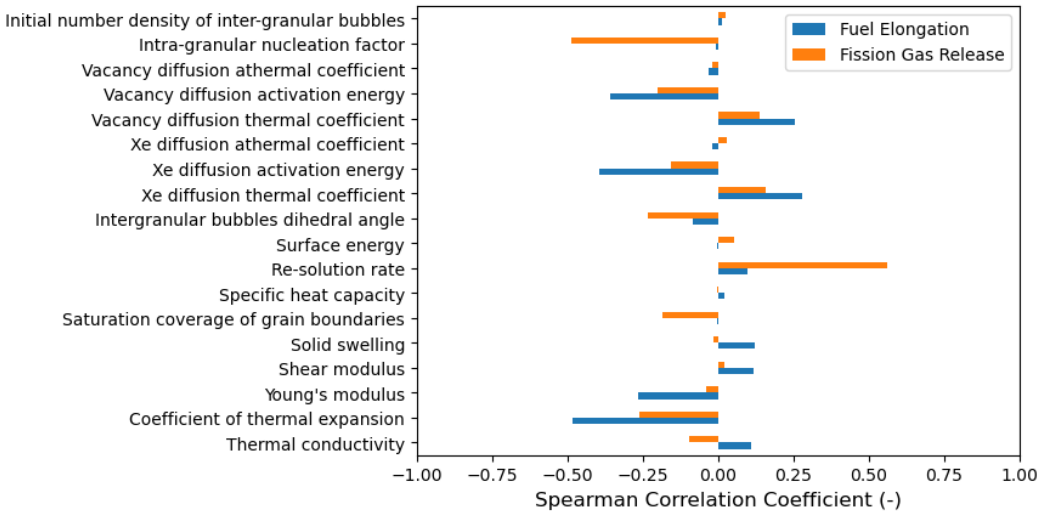

(b)

Figure 3.6. Spearman correlation coefficients using the stoichiometric diffusivities for (a) Rod R4 and (b) Rod R6.

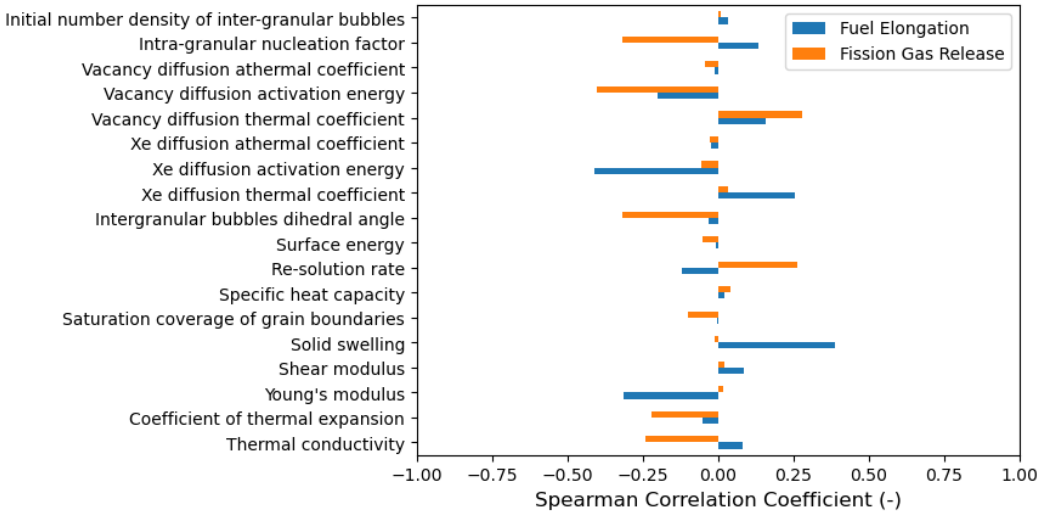

(a)

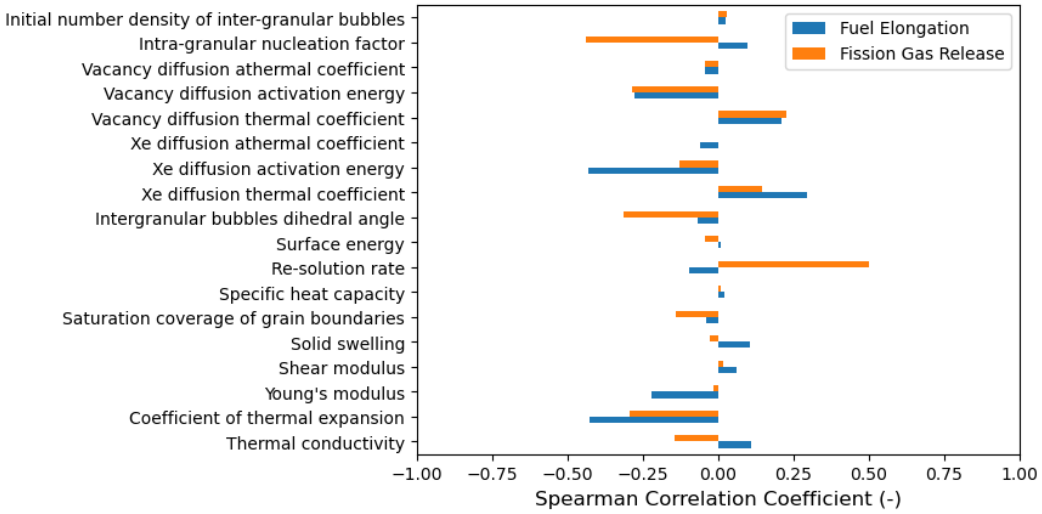

(b)

Figure 3.7. Spearman correlation coefficients using the Si-rich diffusivities for (a) Rod R4 and (b) Rod R6.

4. FeCrAl Cladding

Oxidation-resistant iron-chromium-aluminum (FeCrAl) steels have been proposed for application as cladding materials in light water reactor fuel rods with improved accident tolerance. In addition to improved oxidation resistance, these materials have higher strength and lower creep rates than traditional zirconium-based cladding.

The BISON team began development and implementation of FeCrAl models back in 2015 as part of the ATF high-impact problem (HIP). Since then, the material models have been updated to be consistent with the FeCrAl handbook and any analyses revisited. It is worth noting that the complex of models chosen — or in some cases, developed — for BISON were adopted by the international Coordinated Research Project (CRP) ACTOF of the IAEA [5]. A summary of the fuel performance results for FeCrAl cladding was provided in [30]. The international benchmark, for which INL had a large contribution, through participation in ACTOF, focused on comparing the predicted the fuel performance behavior of FeCrAl during normal operating and accident conditions between multiple fuel performance codes. Despite the material models and operational conditions being explicitly defined, there was large variation amongst the different codes. However, some significant consistency was found between the predictions from BISON and those from two other well-established fuel performance codes, in particular, the European Commisssion's TRANSURANUS code and the FEMAXI-7 code (Japan). Examples of the results from this IAEA benchmark are discussed below.

Modeling problems considered in the benchmark included PWR short fuel rod irradiated under idealized normal operating conditions and cladding-only transient cases for loss of coolant conditions. Five fuel performance codes were applied in the benchmark. Regarding the normal operating conditions case, Figure 4.1 shows the evolution of the hoop stress at the outer surface of the cladding at the axial mid-plane. The cladding is under compression until pellet-clad mechanical interaction (PCMI) is established. The fuel-cladding contact pressure under PCMI results in a reduction of the compressive stresses within the cladding. The point in time at which gap closure occurs is when the slopes of the curves changes abruptly. Reopening of the gap during the final shutdown causes the stress to revert to being compressive under the outer coolant pressure.

Predictions of cladding hoop stress from BISON, FEMAXI-7, and TRANSURANUS in open gap conditions are remarkably consistent with each other. Such agreement is encouraging, especially in view of the significant modeling uncertainties involved in fuel rod analysis and the larger scatter of results observed in

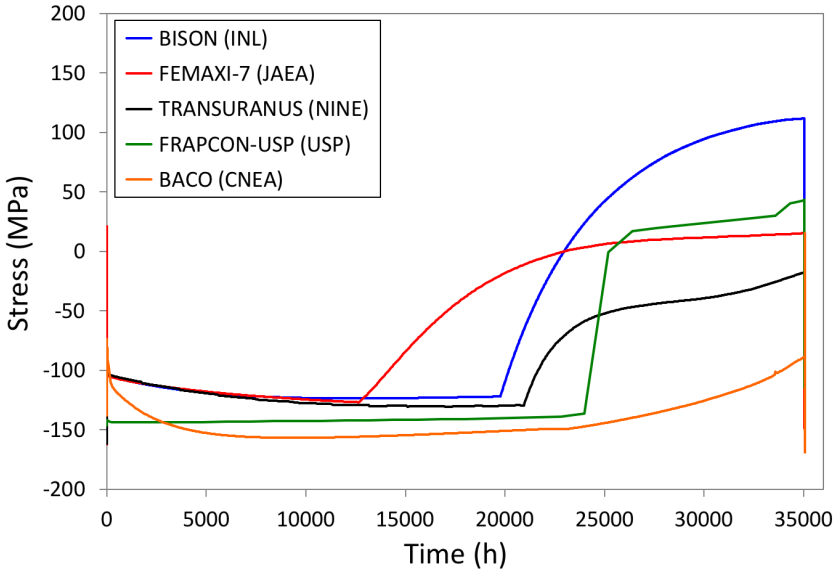

Figure 4.1. Benchmark comparisons between various fuel performance codes for the hoop stress at the outer surface and axial mid-plane of a FeCrAl cladding under PWR normal operating conditions.

previous benchmark exercises that involving more complex fuel rod problems, e.g., [31, 32].

For loss-of-coolant conditions, six cases simulating cladding-only ballooning and burst tests were selected. Benchmark results in terms of time to burst failure are reported in histogram form in Figure 4.2. Experimental data for Zircaloy-4 under the same conditions are also included. Some differences are observed among predictions with different codes. These can be ascribed to differences in the strain calculation and, consequently, in the calculated stress, that determines the burst prediction according to the criterion developed in [33]. However, when comparing the current simulations compared to the experimental data for Zircaloy-4, FeCrAl seems to have a burst resistance similar toZircaloy-4. In addition, FeCrAl is anticipated to be characterized by substantially slower oxidation kinetics, hence less reduction of load bearing capacity due to cladding thinning, as well as a lower hydrogen and heat generation during accident scenarios.

More details on this international benchmark are found in the recently published final report of the IAEA CRP ACTOF [5]. While the international benchmark is not a demonstration of multiscale model development, it is great exposure for the NEAMS program to have the institution (INL) defining and performing the first analyses for an international project.

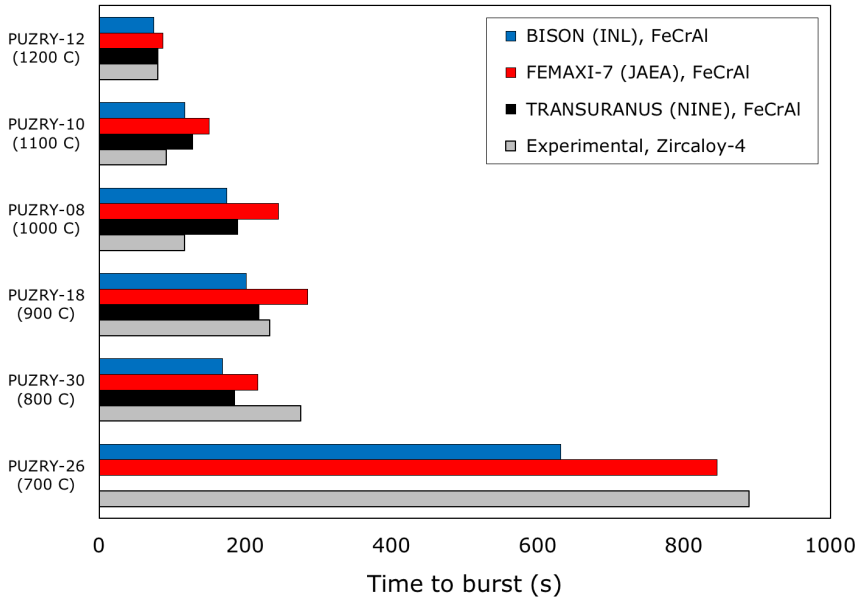

Figure 4.2. Time to cladding burst failure for the loss of coolant cases (PUZRY cases) in the IAEA benchmark. Code-to-code comparisons for FeCrAl and experimental data for Zircaloy-4 under the same conditions, are illustrated.

5. Concluding Remarks

In the beginning, research into ATF concepts was scattered, with a large number of concepts being pursued. More recently, the number of viable concepts has been reduced. Multiscale modeling has provided key insights into the behavior of such concepts which would otherwise many experiments to obtain. Here, the multiscale modeling approach was used to develop fission gas behavior and mechanical models for U_3Si_2 and Cr_2O_3-doped UO_2. This report summarizes the form of the models as implemented into the BISON fuel performance code, with validation to the limited experimental data available. For U_3Si_2, a detailed sensitivity analysis was also completed.

The results indicate that BISON predicts the behavior of Cr_2O_3-doped UO_2 quite well. The updated IFA-681 validation case shows improved predictions compared to those presented with the previous lower length scale model last year [2].

The U_3Si_2 uncertainty and sensitivity analyses show that, because of the large uncertainty in the inputs, the measurements of the ATR-ATF experiments can be captured adequately. A densification model specific to U_3Si_2 would improve fuel elongation predictions.

Since U_3Si_2 is no longer being pursued as an ATF concept, future work will continue to focus on multiscale model development of material properties for doped UO_2, including creep and fracture toughness. These efforts will include the chemical effects of various dopants, where applicable, as well as the effects of the modified microstructure (large grains, different sintered porosity morphology).

FeCrAl is still a front runner among ATF cladding concepts, along with coated zirconium-based cladding. At the lower length scale, work has been completed in developing constitutive laws for FeCrAl [34, 35]. The work identified that the constitutive law could be implemented in the Multiphysics Object-Oriented Simulation Environment (MOOSE)-BISON framework with improved predictions to separate effects failure tests, but was extremely slow. Since then work the LANL team has developed a framework for reduced order models for other materials used as structural materials and cladding in metallic fueled reactors (i.e., HT9). Work has not been completed to create a reduced order model for FeCrAl as of yet. This would be the next step in multiscale modeling of cladding concepts.

6. Publications

The multiscale modeling approach employed by the NEAMS program over the years has led to the preparation, submission and/or acceptance of three journal papers this year. Throughout the report, highlights from these papers have been presented. The three papers include:

1. M. W. D. Cooper, G. Pastore, Y. Che, C. Matthews, A. Forslund, C. R Stanek, K. Shirvan, T. Tverberg, K. A. Gamble, B. Mays, D. A. Andersson, "Fission Gas Diffusion and Release for Cr_2O_3-Doped UO_2: From the Atomic to the Engineering Scale," Journal of Nuclear Materials, (under review).
2. M. W. D. Cooper, K. A. Gamble, K. Metzger, C. Matthews, C. R. Stanek, and D. A. Andersson, "Irradiation enhanced self-diffusion and diffusional creep in U3Si2", (in preparation)
3. K. A. Gamble, G. Pastore, M. W. D. Cooper, D. A. Andersson, B. Beeler, L. K. Aagesen, T. Barani, D. Pizzocri "Integral validation of BISON U_3Si_2 modeling capabilities including multiscale improvements to modeling fission gas behavior," Journal of Nuclear Materials, (under internal review)

Bibliography

[1] R. L. Williamson, K. A. Gamble, D. M. Perez, et al. "Validating the BISON fuel performance code to integral LWR experiments". In: *Nuclear Engineering Design* 301 (2016), pp. 232–244. DOI: 10.1016/j.nucengdes.2016.02.020.

[2] K. A. Gamble et al. *ATF material model development and validation for priority fuel concepts*. Tech. rep. CASL-U-2019-1870-000 Rev.0. Idaho National Laboratory, 2019.

[3] K. A. Gamble. *ATF material model development and validation for priority cladding concepts*. Tech. rep. CASL-U-2019-1892-000 Rev.0. Idaho National Laboratory, 2019.

[4] F. Cappia and J. M. Harp. "Postirradiation examination of low burnup U_3Si_2 fuel for light water reactor applications". In: *Journal of Nuclear Materials* 518 (2019), pp. 62–79.

[5] *Analysis of Options and Experimental Examination of Fuels for Water Cooled Reactors with Increased Accident Tolerance (ACTOF)*. Tech. rep. IAEA-TECDOC-1921. International Atomic Energy Agency, 2020.

[6] J. A. Turnbull et al. "The diffusion coefficients of gaseous and volatile species during the irradiation of uranium dioxide". In: *Journal of Nuclear Materials* 107 (1982), pp. 168–184.

[7] M.W.D. Cooper et al. *Fission Gas Diffusion and Release for Cr_2O_3-Doped UO_2: From the Atomic to the Engineering Scale*. Journal of Nuclear Materials, 2020, accepted.

[8] B. Baurens. *In-pile results from the fission gas release mechanisms study in IFA-716 after final unloading*. Tech. rep. HWR-1161. OECD Halden Reactor Project, 2016.

[9] B. Therache. *The High Initial Rating Test, IFA-677.1: Results after First Cycle of Irradiation*. Tech. rep. HWR-819. OECD Halden Reactor Project, 2005.

[10] R. Josek. *The high initial rating test IFA- 677.1: Final report on in-pile results*. Tech. rep. HWR-872. OECD Halden Reactor Project, 2008.

[11] H. K. Jenssesn. *PIE Report on Six UO2 Fuel Rods Irradiated in IFA-677 High Initial Rating Test*. Tech. rep. HWR-968. OECD Halden Reactor Project, 2010.

[12] J. Klouzal. *Proposal for the testcase for the data validation and treatment*. Presented at the HRP Workshop on F&M Legacy Database, OECD Boulogne-Billancourt, November 19, 2018.

[13] W. Wiesenack. "Verification and improvement of test data for the HRP Legacy Data Base". In: *Enlarged Halden Programme Group Meeting, Sandefjord, Norway, May 19-24, 2019*.

[14] T. Barani et al. "Multiscale modeling of fission gas behavior in U_3Si_2 under LWR conditions". In: *Journal of Nuclear Materials* 522 (2019), pp. 97–110.

[15] L. K. Aagesen et al. "Phase-field simulations of intergranular fission gas bubble behavior in U_3Si_2 nuclear fuel". In: *Journal of Nuclear Materials* 541 (2020), p. 152415. DOI: https://doi.org/10.1016/j.jnucmat.2020.152415.

[16] B. Beeler et al. "Molecular dynamics investigation of grain boundaries and surfaces in U_3Si_2". In: *Journal of Nuclear Materials* 514 (2019), pp. 290–298.

[17] M. W. D. Cooper et al. *Irradiation enhanced diffusion and diffusional creep in U_3Si_2*. Tech. rep. LA-UR-20-24244. Los Alamos National Laboratory, 2020.

[18] R. A. Freeman et al. "Analysis of thermal creep for uranium silicide fuel using Bison". In: *Proceedings of the 2018 International Congress on Advances in Nuclear Power Plants (ICAPP 18)*. Charlotte, NC, 2018.

[19] K. E. Metzger. "Analysis of Pellet Cladding Interaction and Creep of U_3Si_2 Fuel for use in Light Water Reactors". PhD thesis. University of South Carolina, 2016.

[20] J. T. White. *Update to the U_3Si_2 property handbook*. Tech. rep. LA-UR-18-28719. Los Alamos National Laboratory, 2018.

[21] J. M. Harp, P. A. Lessing, and R. E. Hoggan. "Uranium silicide pellet fabrication by powder metallurgy for accident tolerant fuel evaluation and irradiation". In: *Journal of Nuclear Materials* 466 (2015), pp. 728–738.

[22] K. E. Barrett et al. "Critical processes and parameters in the development of accident tolerant fuels drop-in capsule irradiation tests". In: *Nuclear Engineering and Design* 294 (2015), pp. 38–51.

[23] J.L Snelgrove M. R. Finlay G. L. Hofman. "Irradiation behaviour of uranium silicide compounds". In: *Journal of Nuclear Materials* 325 (2004), pp. 118–128.

[24] A. Cheniour et al. "Development of a grain growth model for U_3Si_2 using experimental data, phase field simulation and molecular dynamics". In: *Journal of Nuclear Materials* 532 (2020), p. 152069.

[25] K. E. Metzger, T. W. Knight, and R. L. Williamson. "Model of U_3Si_2 Fuel System using BISON Fuel Code". In: *Proceedings of the International Congress on Advances in Nuclear Power Plants - ICAPP 2014*. Charlotte, NC, 2014.

[26] G. L. Hofman and W. S. Ryu. *Detailed Analysis of Uranium Silicide Dispersion Fuel Swelling*. Tech. rep. CONF-8909141–10. Argonne National Laboratory, 1989.

[27] T. Ikonen and V. Tulkki. "The importance of input interactions in the uncertainty and sensitivity analysis of nuclear fuel behavior". In: *Nuclear Engineering and Design* 275 (2014), pp. 229–241.

[28] B. M. Adams et al. *Dakota, A Multilevel Parallel Object-Oriented Framework for Design Optimization, Parameter Estimation, Uncertainty Quantification, and Sensitivity Analysis: Version 6.11 User's Manual*. Tech. rep. SAND2014-4633. Sandia National Laboratories, 2019.

[29] F. Cappia and J. M. Harp. "Corrigendum to "Postirradiation examination of low burnup U_3Si_2 fuel for light water reactor applications". In: *Journal of Nuclear Materials* 523 (2019), p. 538.

[30] M. Cherubini C. Giovedi A. Marino A. Yamaji Y. Kaji P. Van Uffelen M.S. Veshchunov G. Pastore K.A. Gamble. "Benchmark of Fuel Performance Codes for FeCrAl Cladding Behavior Analysis". In: *Proceedings of TopFuel 2018*. Prague, Czech Republic, 2018.

[31] *Improvement of Computer Codes Used for Fuel Behaviour Simulation (FUMEX-III): Report of a Coordinated Research Project 2008-2012*. Tech. rep. IAEA-TECDOC-1697. International Atomic Energy Agency, 2013.

[32] *Fuel Modelling in Accident Conditions (FUMAC): Final Report of a Coordinated Research Project*. Tech. rep. IAEA-TECDOC-1889. International Atomic Energy Agency, 2019.

[33] K.A. Gamble et al. "An investigation of FeCrAl cladding behavior under normal operating and loss of coolant conditions". In: *Journal of Nuclear Materials* 491 (2017), pp. 55–66.

[34] W. Wen et al. *A physics-based crystallographic modeling framework for describing the thermal creep behavior of Fe-Cr alloys*. Tech. rep. LA-UR-16-27585. Los Alamos National Laboratory, 2017.

[35] A. Patra et al. *Demonstration of finite element simulations in MOOSE using crystallographic models of irradiation hardening and plastic deformation*. Tech. rep. LA-UR-16-23742. Los Alamos National Laboratory, 2016.